

ARTICLE OPEN



Contrasting latitudinal evolution of East Asian monsoonal precipitation during the Last Interglacial (130–120 ka)

Nanxuan Jiang^{1,2}, Qing Yan^{1,3}✉ and Huijun Wang^{1,3}

Evolution of East Asian monsoonal precipitation across the Last Interglacial (LIG) remains controversial, owing to the discrepancies between various proxies and their low temporal resolution. Through a transient high-resolution global climate simulation covering the interval of 130–120 ka, we illustrate a long-term increasing (decreasing) trend in summer precipitation over south China (northeast Asia) during the LIG (i.e. 130–120 ka). The out-of-phase precipitation evolution across latitudes were coherently regulated by the weakened monsoonal circulation, southward moved western North Pacific high, and southward displaced East Asian westerly jet from the early to late LIG. These atmospheric circulation variations were in turn determined by sea surface temperature anomalies over the Pacific and the propagation of extratropical Rossby waves originating from North Africa. Our results may provide important insights for reconciling discrepancies between precipitation proxies during the LIG and for precipitation behavior in a warmer-than-present world.

npj Climate and Atmospheric Science (2024)7:26; <https://doi.org/10.1038/s41612-024-00574-9>

INTRODUCTION

A long-standing issue on East Asian monsoonal precipitation is how it may vary in a future warmer world, given its profound impact on regional ecosystems, human lives, and socioeconomic development^{1–5}. However, there is no consensus on the projected intensity of the East Asian summer monsoon (EASM) and associated precipitation anomaly pattern⁶, partly attributed to the limited understanding of monsoon dynamics that may partially arise from the too-short instrumental observations. Therefore, we may look back into past warm intervals, which could provide insights into mechanistic links between global warming and monsoon variation. In particular, the Last Interglacial (LIG, ~130–115 ka BP) was a naturally induced warmest world driven by Earth's orbit during the past 800 ka, which was witnessed by intense warming over high latitudes (~9 °C over Greenland compared with the preindustrial), reduced glaciers in the polar, and poleward extended boreal forests^{7–12}. These climatic characteristics exhibited profound resemblances to the projected future climates, although with different external forcings^{13–15}. Thus, the LIG has attracted great interest from both data synthesis and numerical modeling over East Asia^{11,13,16,17}.

Geological evidence indicated a generally warmer and wetter condition over East Asia during the LIG^{18–21}, in terms of the mean climate state. However, there has been a hot debate on the temporal evolution of East Asian monsoonal precipitation or EASM across the LIG. One group of records (e.g. stalagmites) suggested a stably stronger state of the EASM between ~130 and 120 ka, followed by an abrupt weakening (Fig. 1b, c)^{22,23}. In contrast, another group of records (e.g., loess sequences and lake sediments) indicated a varied intensity of the East Asian monsoonal precipitation across the LIG, e.g., exhibiting either a long-term increasing or a decreasing trend (Fig. 1d–f)^{19,24–28}. These data–data controversies may arise from the discrepancies in the interpretations of proxies (e.g., speleothem $\delta^{18}\text{O}$), the low temporal resolution, and spatial inconsistency, which may be

resolved via reconstructing precipitation from a single proxy with high-temporal resolution and large latitude span. However, such efforts remain challenging due to great requests for proxies, sites, and techniques. This hence raises a fundamental question: how the East Asian monsoonal precipitation varied across the LIG?

To help address this issue, transient simulations, rather than time-slice experiments, are useful when focusing on the evolution of climate change across the LIG. However, existing transient simulations targeting the LIG^{29–35} may have large uncertainties in depicting East Asian climate, because of the use of orbital acceleration technique³², the simplified physical processes in the intermediate complexity model³⁶, and/or coarse horizontal resolution³⁷. To overcome these limitations, here we performed an transient simulation at high spatial and temporal resolution (i.e., $\sim 1^\circ \times 1^\circ$ without orbital acceleration) from 130 to 120 ka, which was an interval with stably stronger EASM indicated by stalagmites^{22,23}. Our results revealed a divergent evolution of East Asian monsoonal precipitation across latitudes during the LIG, with an increasing (decreasing) trend over south China (northeast Asia) and an indistinctive long-term trend between the two regions. This out-of-phase variation in precipitation was regulated by large-scale atmospheric circulations in summer, which were ultimately driven by the change in May–June–July insolation.

RESULTS

Evolution of monsoonal precipitation across the LIG

East Asian summer monsoonal precipitation exhibited divergent evolutionary patterns across latitudes during 130–120 ka. Comparisons showed that summer terrestrial precipitation had a long-term increasing trend over south China (25–35°N), whereas a decreasing trend was observed over northeast Asia (45–55°N) (Fig. 2). In contrast, precipitation over North China (35–45°N; i.e., between south China and northeast Asia) fluctuated near a basic state during 130–120 ka, without a significant long-term trend (Fig. 2). This was induced by the

¹Nansen-Zhu International Research Centre, Institute of Atmospheric Physics, Chinese Academy of Sciences, Beijing, China. ²University of Chinese Academy of Sciences, Beijing, China. ³Key Laboratory of Meteorological Disaster/Collaborative Innovation Center on Forecast and Evaluation of Meteorological Disasters, Nanjing University of Information Science and Technology, Nanjing, China. ✉email: yanqing@mail.iap.ac.cn

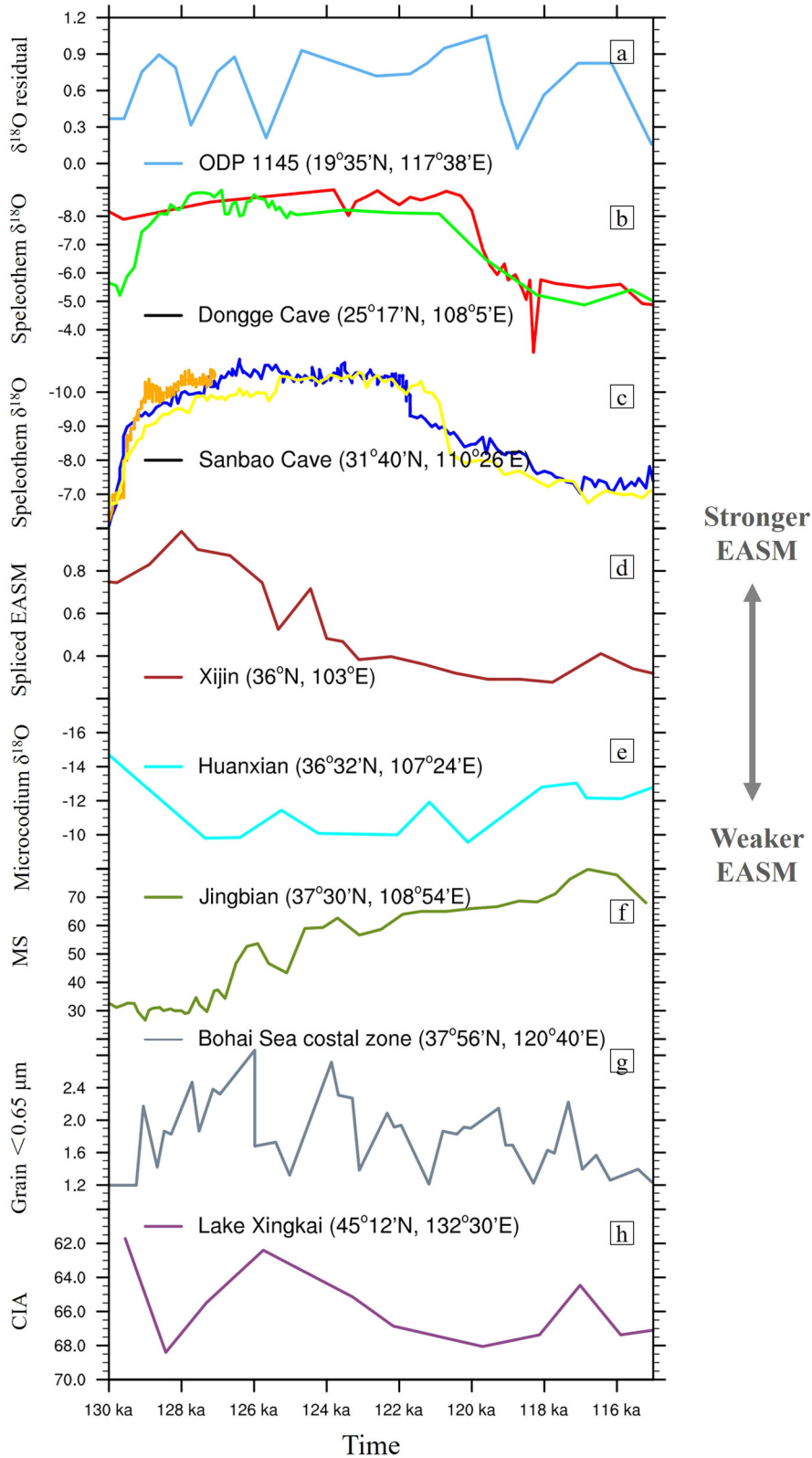


Fig. 1 Evolution of reconstructed East Asian summer monsoon during the LIG based on various proxies. a The residual component of $\delta^{18}\text{O}$ from the Ocean Drill Program Site 1145²⁷. Speleothem $\delta^{18}\text{O}$ data of the stalagmite from the **(b)** Dongge Cave and **(c)** Sanbao Cave^{22,55}. **d** Spliced East Asian summer monsoon (EASM) index derived from the loess records from Xijin, Chinese Loess records²⁵. **e** Microcodium $\delta^{18}\text{O}$ data of the loess records from Huanxian²⁴. **f** Magnetic susceptibility (MS) of the loess records from Jingbian, Chinese Loess Plateau¹⁹. **g** The fraction of grain $<0.63\ \mu\text{m}$ from Miaodao Stratigraphic section²⁸. **h** Chemical Index of Alteration (CIA) of the lake sediments from the Lake Xingkai²⁶.

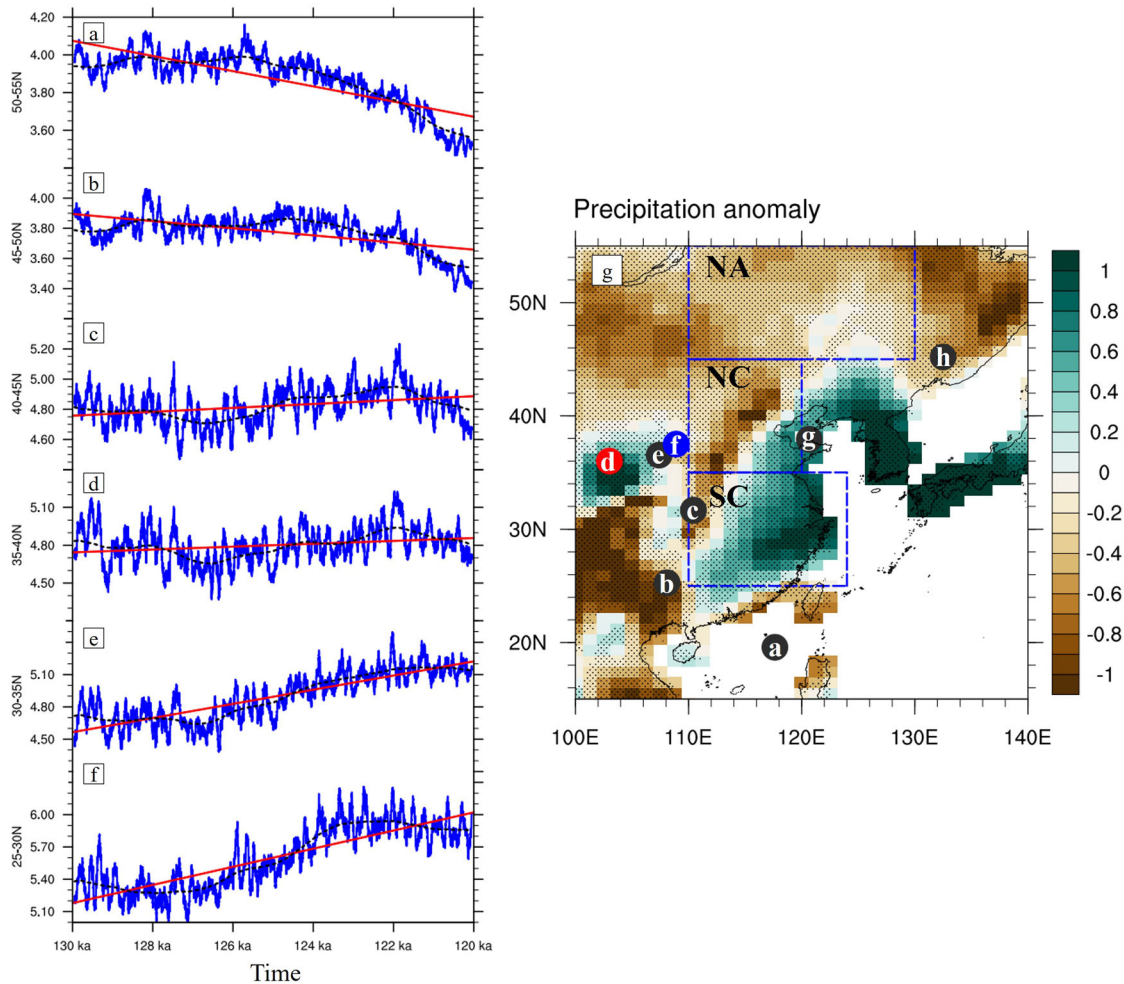


Fig. 2 Variations of summer terrestrial precipitation over East Asia. Evolution of precipitation across different latitude bands during the Last Interglacial (i.e. 130–120 ka) (units: mm d^{-1}) with the latitude bands being (a) 50–55°N, (b) 45–50°N, (c) 40–45°N, (d) 35–40°N, (e) 30–35°N, and (f) 25–30°N. The blue, black, and red lines in (a–f) represent original precipitation evolutions applying a 101-yr running average, their corresponding millennial trends derived from Singular Spectrum Analysis and long-term (130–120 ka) trends, respectively. **g** Anomaly of precipitation over East Asia in summer between 121–120 ka and 130–129 ka (units: mm d^{-1}). The dotted area in (g) represents the difference between 121–120 ka and 130–129 ka passing the significance test at the 95% level. The blue boxes in (g) indicate the region of south China (SC), North China (NC), and northeast Asia (NA), respectively. The blue, red, and gray markers in (g) denote the reconstructed EASM showed a long-term strengthening trend, a long-term weakening trend, and no significant long-term trend, respectively, during 130–120 ka displayed in Fig. 1.

southeastward retreat of the EASM and the resulting opposite variation of precipitation between the west and east of North China (Supplementary Fig. 1). Moreover, the divergent evolution of precipitation was clearly observed in the spatial difference between the late LIG (121–120 ka) and the early LIG (130–129 ka). Precipitation anomalies generally showed a northeast-southwest dipole pattern over the East Asian monsoon domain, with enriched (deficient) amount extending from south China to Japan (pan-northeast Asia), supporting the southeastward retreat of the EASM during the late LIG relative to the early LIG (Fig. 2g). Notably, in addition to the meridional contrast of precipitation, there was a zonal contrast in precipitation change over East Asia, e.g., between the northeastern Tibetan Plateau and the west of North China, which was primarily contributed by the vertical dynamic term (Fig. 2g, Supplementary Fig. 2).

Atmospheric circulations associated with monsoonal precipitation

The differences in summer precipitation between the late and early LIG were closely linked with the variations of atmospheric

circulations. There were anomalous northerly winds over East Asia and cyclonic circulations over Japan during the late LIG relative to the early LIG at 850 hPa (the lower troposphere) (Fig. 3a). This indicated a weakened summer monsoonal circulation during the late LIG, which restricted the northward advance of rainy belt and contributed to increased (decreased) precipitation over south China (northeast Asia). Moreover, the enhanced eddy geopotential height over the North Pacific in the mid-troposphere (500 hPa) suggested a southward retreat of the western North Pacific subtropical high (WNPSH) (Fig. 3b). This also provided favorable conditions for the formation of upward motion over south China, hence resulting in enriched precipitation over there (Figs. 2g, 3d). Moreover, the stronger (weaker) zonal winds over the south (north) of 50°N at 200 hPa showed that the East Asian westerly jet (EAWJ) was intensified and moved more equatorward during the late LIG relative to the early LIG (Fig. 3c). The equatorward located EAWJ can steer transient eddies over south China, supporting increased precipitation over there as well as the reduced precipitation over northeast Asia. The configurations of atmospheric circulation anomalies in the troposphere over East Asia

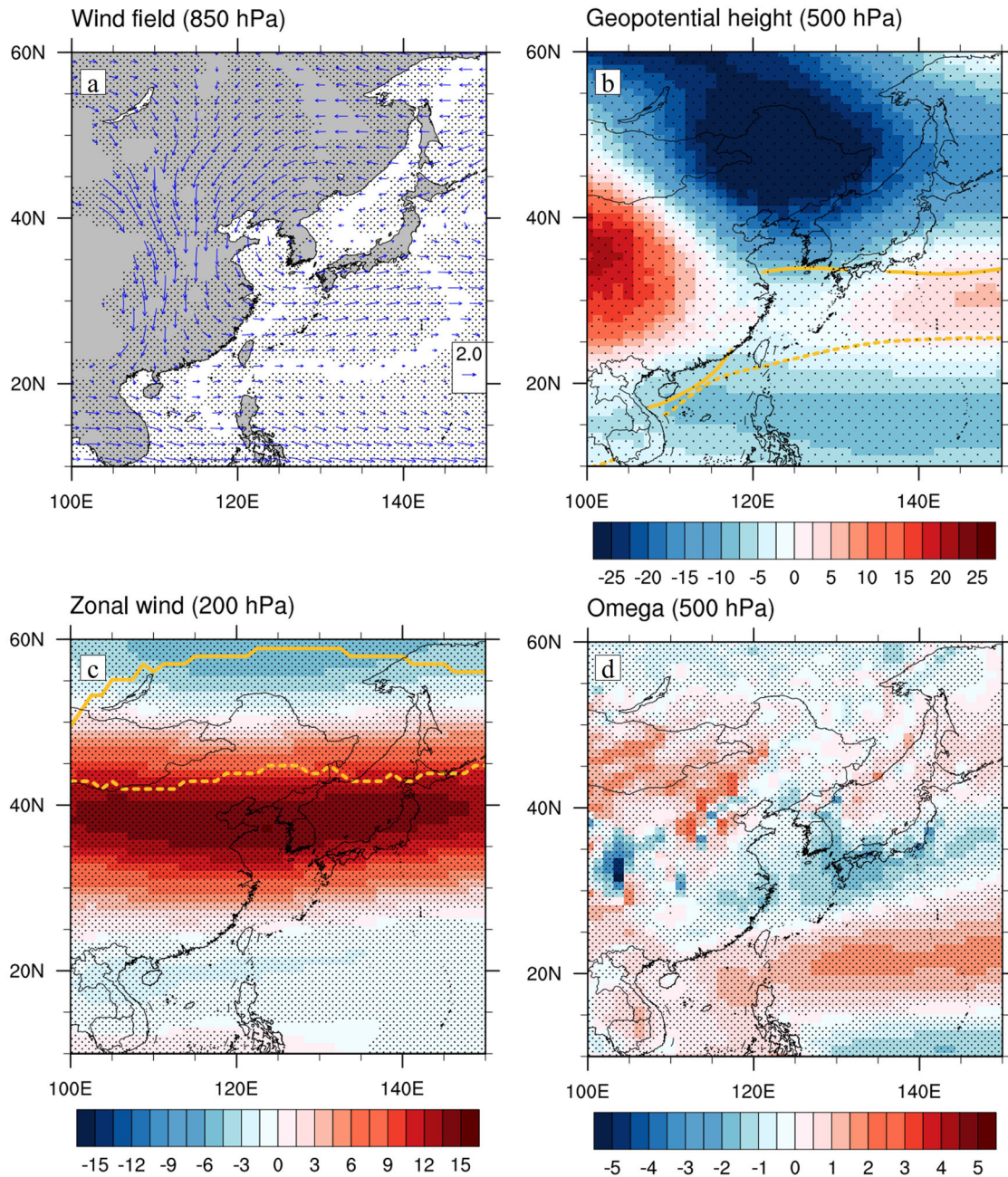


Fig. 3 Changes in atmospheric circulations responsible for variations of precipitation over East Asia in summer during the late LIG relative to the early LIG. Anomaly of (a) wind field at 850 hPa (units: m s^{-1}), (b) eddy geopotential height at 500 hPa by removing the zonal mean (units: gpm), (c) zonal wind at 200 hPa (units: m s^{-1}), and (d) vertical velocity at 500 hPa (units: 0.01 Pa s^{-1}) between 121–120 ka and 130–129 ka. Orange solid and dotted lines in (b) represent the zero line of zonal wind at 500 hPa to indicate the location of the western North Pacific subtropical high during 130–129 ka and 121–120 ka, respectively. Orange solid and dotted lines in (c) represent the jet axis of the East Asian westerly jet during 130–129 ka and 121–120 ka, respectively. The dotted area in (a–d) represents the difference between 121–120 ka and 130–129 ka passing the significance test at the 95% level.

gave rise to anomalous upward (downward) motions over south China (northeast Asia) in the non-divergence level (i.e. 500 hPa) during the late LIG relative to the early (Fig. 3d), and ultimately resulted in the northeast-southwest dipole pattern of precipitation over East Asia.

The alternations in atmospheric circulations as well as the precipitation anomalies over East Asia are in turn tied to the adjustment of the atmospheric thermal structure and the associated climatic changes. The cooling over the East Asian inland was more intense than over south China and the subtropical Pacific during the late relative to the early LIG (Fig. 4a,

Supplementary Fig. 3). This was associated with increased surface pressure over Asian inland and decreased one over south China and the subtropical Pacific, which weakened the north-south pressure gradient and resulted in the northerly winds over East Asia (Fig. 4a). Moreover, the reduced meridional gradient of sea surface temperature (SST) over the North Pacific, manifested by anomalous warming over the north of Taiwan and cooling over the south. This was disadvantage for the northward location of the WNPSH (Fig. 4d), similar to the casual relationship observed in modern climate³⁸. The anomalous anticyclone (cyclone) over south China and cyclone (northeast Asia) at 200 hPa resulted in the

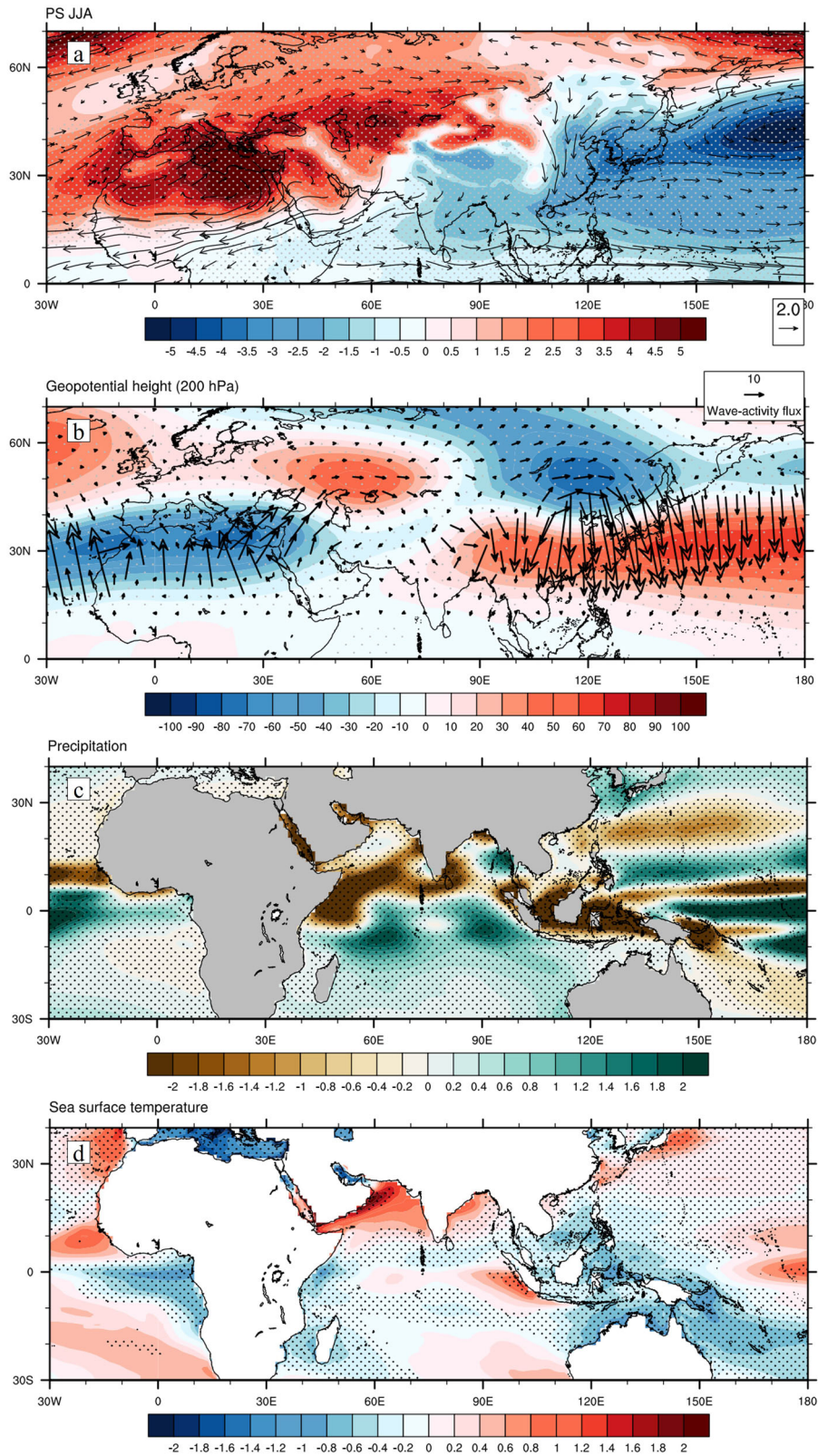


Fig. 4 Large scale climatic changes during the late LIG relative to the early LIG. Anomaly of (a) surface pressure (shade, units: hPa) and wind field (vector, units: m s^{-1}) at 850 hPa, (b) eddy geopotential height by removing the zonal mean (shade, units: gpm) and wave activity flux (vector, units: $\text{m}^2 \text{s}^{-2}$) at 200 hPa, (c) precipitation (units: mm d^{-1}), and (d) eddy sea surface temperature by removing the zonal mean (units: °C) between 121–120 ka and 130–129 ka. The dotted area represents the difference between 121–120 ka and 130–129 ka passing the significance test at the 95% level.

southward displacement of the EAWJ (Fig. 4b). The configuration of anticyclonic circulation at 200 hPa and cyclonic circulation at 850 hPa over south China suggested a baroclinic structure (Fig. 4a, b). Based on the Matsuno–Gill response, the anticyclone/cyclone may be partially induced by increased precipitation over its southeastern flank near the east of the Philippines arising from the increased SST over there (Fig. 4c, d). These results indicated the important roles of changes in the SSTs during the late LIG relative to the early in regulating the precipitation-associated atmospheric circulations over East Asia. Additionally, in the upper troposphere, the extratropical Rossby waves originated from North Africa and then propagated northeastward to Central Asia (Fig. 4b). Then the wave train branched two pathways, with the major one propagating eastward and turning southward to south China and the other propagating southeastward directly (Fig. 4b). This suggested that the horizontal propagation of extratropical Rossby waves was likely to play a role in the formation of the anomalous atmospheric circulations over East Asia. Overall, variations of SSTs over the subtropical/North Pacific and the propagation of extratropical Rossby waves jointly regulated anomalous atmospheric circulations over East Asia during the late LIG relative to the early.

Moisture budget analysis for monsoonal precipitation

Moreover, we utilized the moisture budget analysis to further estimate the contributions of dynamic and thermodynamic processes in precipitation variations over East Asia across the LIG (Fig. 5). The horizontal thermodynamic term and the vertical dynamic term played the most important role in determining increased precipitation over south China, with the positive contribution from the horizontal dynamic term. In contrast, all the evaporation, horizontal and vertical thermodynamic/dynamic terms were essential in resulting in decreased precipitation over northeast Asia. This highlighted that the variations of atmospheric circulations and reduced specific humidity (Supplementary Fig. 4) were both important in regulating precipitation over there during the late LIG relative to the early. In addition, over the transition zone (North China), the decreased precipitation over the western part was dominated by evaporation, vertical dynamic, vertical thermodynamic, and non-linear terms, whereas the increased precipitation over the east was controlled by the horizontal thermodynamic and vertical dynamic terms (Supplementary Fig. 5). Notably, the residual term was relatively larger in the moisture budget analysis during the late LIG relative to the early, which may arise from the non-negligible difference of the moisture storage in

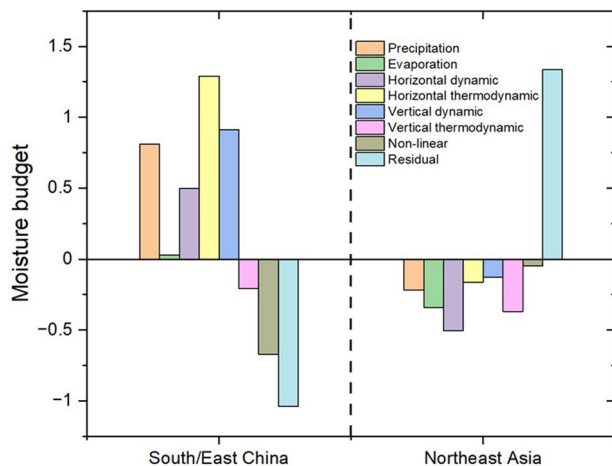


Fig. 5 Moisture budget analysis over South/East China (25–40°N, 115–130°E) and northeast Asia (40–55°N, 110–130°E) between 121–120 ka and 130–129 ka (units: mm d^{-1}).

the atmosphere due to the mean climate state discrepancies, and was also found in previous modeling studies^{39,40}.

DISCUSSIONS

Here, we reveal a divergent evolution of East Asian monsoonal precipitation across latitudes during the LIG, with an increasing (decreasing) trend over south China (northeast Asia) and an indistinctive long-term trend between the two regions (Fig. 2). We speculate that the out-of-phase variations of precipitation over south China and northeast Asia may follow the variation of orbital insolation in May–June–July during the LIG (Fig. 6). Specifically, insolation in May–June–July over East Asia increased from 130 to 128 ka and then decreased profoundly (Supplementary Fig. 6). Decreased May–June–July solar insolation determined the cooling trend in summer over East Asia during the LIG (Supplementary Fig. 7), due to the delayed effect of solar insolation on climate change. The decreased temperature over East Asia was not uniform, with more remarkable cooling over the land at mid-high latitudes than over the ocean at low latitudes, induced by the land-sea thermal contrast (Supplementary Fig. 7). This led to weakened monsoonal circulations and the southeastward retreat of the EASM (Supplementary Fig. 8), which further resulted in the long-term decreasing trend over northeast Asia and an increasing precipitation trend over south China during the LIG. Overall, our results highlighted out-of-phase changes in simulated East Asian monsoonal precipitation across East Asia in response to the precession.

We notice that the responses of East Asian monsoonal precipitation are complicated in a warmer world, which are dependent on the external forcings inducing the warmth. In the transition from the early LIG (warm) to late LIG (relatively cold), we reveal the out-of-phase variations of East Asian monsoonal precipitation over south China and northeast Asia across the LIG, in tandem with the weakened EASM. This was also observed during the Holocene (~11–0 ka), with May–June–July insolation also characterized by a general decreasing trend^{41,42}. In contrast, in an increased greenhouse gas dominated warmer world, an increasing trend in East Asian monsoonal precipitation has been

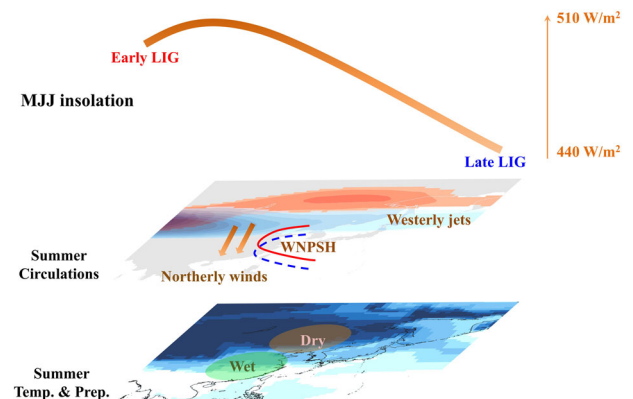


Fig. 6 Schematic diagram of the role of May–June–July solar insolation in driving variations of atmospheric circulations and associated precipitation pattern during the late LIG relative to the early LIG in summer. The shade pattern and circles at the bottom denote surface temperature and precipitation anomalies between the late LIG and early LIG in summer, respectively. The shade in the middle represents the zonal wind/the location of the westerly jet during the early LIG (red) and late LIG (blue) in summer. The red and blue contour in the middle represents the location of the western North Pacific subtropical high (WNPSH) during the early LIG and late LIG in summer, respectively. The vector in the middle indicates the anomaly of meridional wind during the late LIG relative to the early LIG in summer. The curve at the top indicates the evolution of May–June–July solar insolation at 25–55°N between 130 ka and 120 ka.

projected⁴, whereas a dipole anomaly pattern was observed during the warm mid-Pliocene (~3.0 Ma characterized by elevated CO₂ concentration (~400 ppm)⁴³. This highlights the complexity of variations in the EASM and associated precipitation in a warmer-than-present world, in tandem with mechanistic links between global warming and monsoon change. It should be noted that although the external forcings and associated precipitation responses are different between the LIG and the future, the profound warming over the mid-high latitudes is similar^{7,13}, in tandem with the strengthened monsoonal circulations relative to the present day^{5,40}. Therefore, understanding changes in the EASM during the LIG may be indicative of its behavior in a future warmer world to some extent.

Given that the reconstructed precipitation over East Asia varied across sites and proxies, it was a matter of course that our simulated results were consistent with some proxies (e.g.^{25,26,44}), but still contradicted with others (e.g.^{24,28}). Therefore, a future study that reconstructs precipitation from a single proxy with high-temporal resolution and a large latitude span together with a series of transient simulations needs to be carried out to better decipher the evolution of East Asian monsoonal precipitation during the LIG. Nevertheless, we provide a modeled scenario on the evolution of East Asian monsoonal precipitation across the LIG. This may have important implications for reconciling the discrepancies in the reconstructed precipitation across proxies/sites and shed light on precipitation behavior in a warmer-than-present world.

METHODS

Model and experimental setups

We use the Community Earth System Model (CESM) version 1.2.2 to perform a Transient Global Climate Simulation covering the LIG (i.e., 130 to 120 ka) (hereafter referred to TGCS-LIG). The CESM is a fully coupled global climate model that has interactive flux among the atmosphere, ocean, land, and sea ice components⁴⁵. In this study, we perform the TGCS-LIG at f09g16 resolution. The Community Atmosphere Model version 4 (CAM4) has a horizontal resolution of ~0.9° × 1.25° with 26 hybrid coordinate vertical levels, and the horizontal resolution of the Community Land Model version 4 (CLM4) is identical to the CAM4. The Parallel Ocean Program version 2 (POP2) with 60 vertical levels and the Community Ice CodE version 4 (CICE) are at ~1° horizontal resolution. The CESM1.2 well reproduces the modern spatial pattern of East Asian monsoonal precipitation compared with the observations, with the spatial correlation coefficient and root-mean-square error of 0.98 and ~0.45 mm d⁻¹, respectively (Supplementary Fig. 9). We perform the TGCS-LIG experiment using 384 cores on a Linux cluster supercomputer, with a throughput of ~18 model years per wall-clock day. For the 10,000 model years, the TGCS-LIG experiment costs ~5.5 million core-hours and produces ~166 TB of outputs.

To perform the TGCS-LIG experiment, we first carry out an equilibrium run at 130 ka (LIG_130 ka), which serves as the initial condition for the TGCS-LIG experiment. In the LIG_130 ka experiment, orbital parameters are set to the levels of 130 ka based on Berger⁴⁶ and greenhouse gas concentrations use the mean value between 130.5–129.5 ka according to Köhler et al.⁴⁷ (Supplementary Table 1). Ice sheets and vegetation in the LIG_130 ka are kept the same as the preindustrial conditions. The LIG_130 ka experiment is branched off from a 1300-year long-time picontrol experiment⁴⁸, in which the last 100-yr annual net radiation at the top of the atmosphere shows no long-term trend (~0.0002 W m⁻² yr⁻¹). The LIG_130 ka experiment is then integrated for additional 450 years to allow the surface climate to reach quasi-equilibrium (i.e., net radiation at

the top of the atmosphere averaged over the last 100 years is ~0.0001 W m⁻² yr⁻¹).

Next, the TGCS-LIG experiment is initialized from the LIG_130 ka experiment and integrated for another 10,000 years (i.e., from 130 to 120 ka). Regarding the external forcings, orbital parameters are adopted from Berger⁴⁶, and greenhouse gas concentrations are obtained from Köhler et al.⁴⁷, following the guidelines of the PMIP4⁴⁹. Briefly, July solar insolation at 25°N increases since 130 ka, reaches the peak at ~125 ka, and then decreases afterward (Supplementary Fig. 10a). Atmospheric CO₂ increases rapidly since 129 ka and then drops, with slight fluctuations since 128 ka (Supplementary Fig. 10b). The evolution of atmospheric CH₄ is similar to that of atmospheric CO₂ (Supplementary Fig. 10c), whereas atmosphere N₂O generally shows an increasing trend during 130–120 ka (Supplementary Fig. 10d). Besides, all the other boundary conditions are kept the same as the preindustrial (e.g., ice sheets and vegetation). Although the roles of ice sheets and vegetation were neglected in the TGCS-LIG experiment, they may have limited impact on the temporal evolution of the East Asian monsoonal precipitation, but influence the changing magnitude, as indicated in previous studies^{50,51}.

Extratropical and tropical Rossby waves

We use the wave-activity flux (\mathbf{W}) to indicate the horizontal propagation direction of Rossby waves⁵², which is defined as:

$$\mathbf{W} = \frac{1}{2|\bar{U}|} \begin{bmatrix} \bar{u}(\psi_x'^2 - \psi' \psi_{xx}') + \bar{v}(\psi_x' \psi_y' - \psi' \psi_{xy}') \\ \bar{u}(\psi_x' \psi_y' - \psi' \psi_{xy}') + \bar{v}(\psi_y'^2 - \psi' \psi_{yy}') \end{bmatrix} \quad (1)$$

where u is the zonal wind velocities, and v is the meridional wind velocities. ψ stands for the stream function. Here, the overbar indicates the mean climate state during 130–120 ka, and the prime indicates the differences between the late LIG (121–120 ka) and the early LIG (130–129 ka).

Additionally, the barotropic structure of the anomalous circulations (i.e. a cyclone in the lower troposphere accompanied by a cyclone in the upper troposphere; and vice versa for the anticyclone) may primarily result from the propagation of extratropical Rossby waves. In contrast, the baroclinic structure of the anomalous circulations may arise from anomalous diabatic heating/cooling over the tropics, indicated by anomalous cyclone (anticyclone) in the lower (upper) troposphere over the north-western flank of the heating source in the Northern Hemisphere based on the Matsuno–Gill response^{53,54}; and vice versa for the diabatic cooling.

Moisture budget analysis

We use the moisture budget formulation to analyze the relative contribution of dynamic and thermodynamic terms in regulating summer precipitation over East Asia during 130–120 ka. The moisture budget relationship is defined as:

$$P' = -\langle \bar{w} \partial_p q' \rangle - \langle w' \partial_p \bar{q} \rangle - \langle \bar{\mathbf{V}} \cdot \nabla q' \rangle - \langle \mathbf{V}' \cdot \nabla \bar{q} \rangle - \langle w' \partial_p q' \rangle - \langle \mathbf{V}' \cdot \nabla q' \rangle + E' + \delta \quad (2)$$

where P stands for the precipitation, and q represents the specific humidity. \mathbf{V} is the horizontal velocity vector, and E is on behalf of the evaporation. δ indicates the residual term. The overbar indicates the climatology between 130 and 120 ka, and the prime indicates the differences between the late LIG (121–120 ka) and the early LIG (130–129 ka). Term $-\langle \bar{w} \partial_p q' \rangle$, $-\langle w' \partial_p \bar{q} \rangle$, $-\langle \bar{\mathbf{V}} \cdot \nabla q' \rangle$ and $-\langle \mathbf{V}' \cdot \nabla \bar{q} \rangle$ indicates the vertical thermodynamic term, vertical dynamic term, horizontal thermodynamic term, and horizontal dynamic term, respectively. Term $-\langle w' \partial_p q' \rangle$ and $-\langle \mathbf{V}' \cdot \nabla q' \rangle$ stand for non-linear terms. Variations of humidity dominate the thermodynamic processes, whereas atmospheric circulation changes (i.e. velocity anomalies) control the dynamic processes.

DATA AVAILABILITY

The related variables of the TGCS-LIG experiment used in this study are available on Zendo: <https://doi.org/10.5281/zenodo.10472824>.

Received: 24 August 2023; Accepted: 11 January 2024;

Published online: 23 January 2024

REFERENCES

- Chen, F. H. et al. Stable East Asian monsoon climate during the Last Interglacial (Eemian) indicated by paleosol S1 in the western part of the Chinese Loess Plateau. *Glob. Planet. Change* **36**, 171–179 (2003).
- Ding, Y. & Chan, J. C. L. The East Asian summer monsoon: an overview. *Meteorol. Atmos. Phys.* **89**, 117–142 (2005).
- Ding, Y., Liu, Y. & Hu, Z. Z. The Record-breaking Meiyu in 2020 and Associated Atmospheric Circulation and Tropical SST Anomalies. *Adv. Atmos. Sci.* **38**, 1980–1993 (2021).
- Li, J. et al. Future precipitation changes in three key sub-regions of East Asia: the roles of thermodynamics and dynamics. *Clim. Dyn.* **59**, 1377–1398 (2021).
- He, C. & Zhou, W. Different enhancement of the east asian summer monsoon under global warming and interglacial epochs simulated by CMIP6 models: role of the subtropical high. *J. Clim.* **33**, 9721–9733 (2020).
- Lee, J.-Y. et al. Future Global Climate: Scenario-Based Projections and Near-Term Information. In *Climate Change 2021: The Physical Science Basis. Contribution of Working Group I to the Sixth Assessment Report of the Intergovernmental Panel on Climate Change* [Masson-Delmotte, V. et al. (eds.)], Cambridge University Press, Cambridge, United Kingdom and New York, NY, USA, 553–672 (2021).
- Turney, C. S. M. et al. A global mean sea-surface temperature dataset for the Last Interglacial (129–116 kyr) and contribution of thermal expansion to sea-level change. *Earth Syst. Sci. Data* **12**, 3341–3356 (2020).
- Hoffman, J. S., Clark, P. U., Parnell, A. C. & He, F. Regional and global sea-surface temperatures during the last interglaciation. *Science* **355**, 276–279 (2017).
- Dutton, A. et al. Sea-level rise due to polar ice-sheet mass loss during past warm periods. *Science* **349**, aaa4019 (2015).
- Stone, E. J., Lunt, D. J., Annan, J. D. & Hargreaves, J. C. Quantification of the Greenland ice sheet contribution to Last Interglacial sea level rise. *Clim. J.* **9**, 621–639 (2013).
- Past Interglacials Working Group of PAGES. Interglacials of the last 800,000 years. *Rev. Geophys.* **54**, 162–219 (2016).
- O’ishi, R. et al. PMIP4/CMIP6 last interglacial simulations using three different versions of MIROC: importance of vegetation. *Clim. J.* **17**, 21–36 (2021).
- Gulev, S. K. et al. Changing State of the Climate System. In *Climate Change 2021: The Physical Science Basis. Contribution of Working Group I to the Sixth Assessment Report of the Intergovernmental Panel on Climate Change* [Masson-Delmotte, V. et al. (eds.)], Cambridge University Press, Cambridge, United Kingdom and New York, NY, USA, 287–422 (2021).
- DeConto, R. M. & Pollard, D. Contribution of Antarctica to past and future sea-level rise. *Nature* **531**, 591–597 (2016).
- Yuan, W. et al. Projecting Future Vegetation Change for Northeast China Using CMIP6 Model. *Remote Sens.* **13**, 3531 (2021).
- Otto-Bliesner, B. L. et al. The PMIP4 contribution to CMIP6 – Part 2: Two interglacials, scientific objective and experimental design for Holocene and Last Interglacial simulations. *Geosci. Model Dev.* **10**, 3979–4003 (2017).
- Capron, E. et al. Critical evaluation of climate syntheses to benchmark CMIP6/PMIP4 127 ka Last Interglacial simulations in the high-latitude regions. *Quat. Sci. Rev.* **168**, 137–150 (2017).
- Cheng, H. et al. The Asian monsoon over the past 640,000 years and ice age terminations. *Nature* **534**, 640 (2016).
- Stevens, T. et al. Ice-volume-forced erosion of the Chinese Loess Plateau global Quaternary stratotype site. *Nat. Commun.* **9**, 983 (2018).
- Tang, C. et al. Tropical and high latitude forcing of enhanced megadroughts in Northern China during the last four terminations. *Earth Planet. Sc. Lett.* **479**, 98–107 (2017).
- Nakagawa, T. et al. Regulation of the monsoon climate by two different orbital rhythms and forcing mechanisms. *Geology* **36**, 491–494 (2008).
- Yuan, D. et al. Timing, Duration, and Transitions of the Last Interglacial Asian Monsoon. *Science* **304**, 575–578 (2004).
- Liu, G. et al. On the glacial-interglacial variability of the Asian monsoon in speleothem $\delta^{18}\text{O}$ records. *Sci. Adv.* **6**, eaay8189 (2020).
- Zhang, Z. et al. Variation of summer precipitation $\delta^{18}\text{O}$ on the Chinese Loess Plateau since the last interglacial. *J. Quat. Sci.* **36**, 1214–1220 (2021).
- Guo, B. et al. Dominant precessional forcing of the East Asian summer monsoon since 260 ka. *Geology* **50**, 1372–1376 (2022).
- Sun, W. et al. Linkage between Lake Xingkai sediment geochemistry and Asian summer monsoon since the last interglacial period. *Palaeogeogr. Palaeoclimatol. Palaeoecol.* **512**, 71–79 (2018).
- Oppo, D. W. & Sun, Y. Amplitude and timing of sea-surface temperature change in the northern South China Sea: Dynamic link to the East Asian monsoon. *Geology* **33**, 785–788 (2005).
- Du, S. et al. East Asian Monsoon Precipitation and Paleoclimate Record Since the Last Interglacial Period in the Bohai Sea Coastal Zone, China. *Terr. Atmos. Ocean. Sci.* **27**, 825–836 (2016).
- Yin, Q. et al. Insolation triggered abrupt weakening of Atlantic circulation at the end of interglacials. *Science* **373**, 1035–1040 (2021).
- Sommers, A. N. et al. Retreat and Regrowth of the Greenland Ice Sheet During the Last Interglacial as Simulated by the CESM2-CISM2 Coupled Climate–Ice Sheet Model. *Palaeogeogr. Palaeoclimatol.* **36**, e2021PA004272 (2021).
- Govin, A., Varma, V. & Prange, M. Astronomically forced variations in western African rainfall (21°N–20°S) during the Last Interglacial period. *Geophys. Res. Lett.* **41**, 2117–2125 (2014).
- Varma, V., Prange, M. & Schulz, M. Transient simulations of the present and the last interglacial climate using the Community Climate System Model version 3: effects of orbital acceleration. *Geosci. Model Dev.* **9**, 3859–3873 (2016).
- Li, X. et al. Transient simulation of orbital-scale precipitation variation in monsoonal East Asia and arid central Asia during the last 150 ka. *J. Geophys. Res. Atmos.* **118**, 7481–7488 (2013).
- Bakker, P. et al. Last interglacial temperature evolution—a model inter-comparison. *Clim. J.* **9**, 605–619 (2013).
- Bakker, P. et al. Temperature trends during the Present and Last Interglacial periods – a multi-model-data comparison. *Quat. Sci. Rev.* **99**, 224–243 (2014).
- Nikolova, I. et al. The last interglacial (Eemian) climate simulated by LOVECLIM and CCSM3. *Clim. J.* **9**, 1789–1806 (2013).
- Tong, Y. et al. Bias correction of temperature and precipitation over China for RCM simulations using the QM and QDM methods. *Clim. Dyn.* **57**, 1425–1443 (2020).
- He, C. et al. Enhanced or weakened western north pacific subtropical high under global warming? *Sci. Rep.* **5**, 16771 (2015).
- Sun, Y. et al. The contrasting effects of thermodynamic and dynamic processes on East Asian summer monsoon precipitation during the Last Glacial Maximum: a data-model comparison. *Clim. Dyn.* **56**, 1303–1316 (2020).
- Jiang, N., Yan, Q. & Wang, H. General characteristics of climate change over China and associated dynamic mechanisms during the Last Interglacial based on PMIP4 simulations. *Glob. Planet. Change* **208**, 103700 (2021).
- Shi, J. & Yan, Q. Evolution of the Asian–African Monsoonal Precipitation over the last 21 kyr and the Associated Dynamic Mechanisms. *J. Clim.* **32**, 6551–6569 (2019).
- Wang, J., Cheng, J. & Lu, H. Comparative analysis of simulation and reconstruction of climate change in the south and north of the East Asian summer monsoon region over the last 21 ka (in Chinese). *Quat. Sci.* **39**, 589–601 (2019).
- Zhang, R. et al. Modeling the late Pliocene global monsoon response to individual boundary conditions. *Clim. Dyn.* **53**, 4871–4886 (2019).
- Iwamoto, N. & Inouchi, Y. Reconstruction of millennial-scale variations in the East Asian summer monsoon over the past 300 ka based on the total carbon content of sediment from Lake Biwa, Japan. *Environ. Geol.* **52**, 1607–1616 (2007).
- Hurrell, J. W. et al. The community earth system model: a framework for collaborative research. *B. Am. Meteorol. Soc.* **94**, 1339–1360 (2013).
- Berger, A. L. Long-term variations of daily insolation and Quaternary climatic changes. *J. Atmos. Sci.* **35**, 2362–2367 (1978).
- Köhler, P. et al. A 156 kyr smoothed history of the atmospheric greenhouse gases CO_2 , CH_4 , and N_2O and their radiative forcing. *Earth Syst. Sci. Data* **9**, 363–387 (2017).
- Schurer, A. P. et al. Disentangling the causes of the 1816 European year without a summer. *Environ. Res. Lett.* **14**, 094019 (2019).
- Menviel, L. et al. The penultimate deglaciation: protocol for Paleoclimate Modelling Intercomparison Project (PMIP) phase 4 transient numerical simulations between 140 and 127 ka, version 1.0. *Geosci. Model Dev.* **12**, 3649–3685 (2019).
- Lyu, A. & Yin, Q. The spatial-temporal patterns of East Asian climate in response to insolation, CO_2 and ice sheets during MIS-5. *Quat. Sci. Rev.* **293**, 107689 (2022).
- Zhang, Q. & Chen, J. Enhanced East Asian summer monsoon precipitation due to vegetation feedback during the last interglacial 127 ka (in Chinese). *Quat. Sci.* **40**, 1499–1512 (2020).
- Takaya, K. & Nakamura, H. A formulation of a phase-independent wave-activity flux for stationary and migratory quasigeostrophic eddies on a zonally varying basic flow. *J. Atmos. Sci.* **58**, 608–627 (2001).
- Matsuno, T. Quasi-Geostrophic Motions in the Equatorial Area. *J. Meteorol. Soc. Jpn.* **44**, 25–43 (1966).
- Gill, A. E. Some simple solutions for heat-induced tropical circulation. *Q. J. Roy. Meteor. Soc.* **106**, 447–462 (1980).
- Wang, Y. et al. Millennial- and orbital-scale changes in the East Asian monsoon over the past 224,000 years. *Nature* **451**, 1090 (2008).

ACKNOWLEDGEMENTS

This study was funded by the National Natural Science Foundation of China (42221004), the Second Tibetan Plateau Scientific Expedition and Research program (2019QZKK010) and the Youth Innovation Promotion Association by CAS (Q. Yan).

AUTHOR CONTRIBUTIONS

N.J. organized the outline, developed the methodology, performed the experiment, provided figures and wrote the manuscript. Q.Y. conceived the presented idea and wrote the manuscript. H.W. provided suggestions and wrote the manuscript.

COMPETING INTERESTS

The authors declare no competing interests.

ADDITIONAL INFORMATION

Supplementary information The online version contains supplementary material available at <https://doi.org/10.1038/s41612-024-00574-9>.

Correspondence and requests for materials should be addressed to Qing Yan.

Reprints and permission information is available at <http://www.nature.com/reprints>

Publisher's note Springer Nature remains neutral with regard to jurisdictional claims in published maps and institutional affiliations.



Open Access This article is licensed under a Creative Commons Attribution 4.0 International License, which permits use, sharing, adaptation, distribution and reproduction in any medium or format, as long as you give appropriate credit to the original author(s) and the source, provide a link to the Creative Commons license, and indicate if changes were made. The images or other third party material in this article are included in the article's Creative Commons license, unless indicated otherwise in a credit line to the material. If material is not included in the article's Creative Commons license and your intended use is not permitted by statutory regulation or exceeds the permitted use, you will need to obtain permission directly from the copyright holder. To view a copy of this license, visit <http://creativecommons.org/licenses/by/4.0/>.

© The Author(s) 2024